Catalysis Letters (2019) 149:1856–1863
https://doi.org/10.1007/s10562-019-02789-5

# MgO Modifying $Al_2O_3$ to Load Cobalt Oxide for Catalytic $N_2O$ Decomposition

**Ye Li[1] · Xinping Wang[1]**

Received: 27 February 2019 / Accepted: 8 April 2019 / Published online: 22 April 2019


## Abstract

Alumina modified by MgO as the catalyst support loading $Co_3O_4$ for the $N_2O$ decomposition were investigated. It was found that $MgAl_2O_4$ was formed over the alumina surface by the MgO reacting with $Al_2O_3$ after calcination at 900 °C and using the composited support containing 30 wt% MgO loading $Co_3O_4$ can effectively suppress undesired $CoAl_2O_4$ formation under 700 °C. In the 20Co/30Mg–Al catalyst, it was found that about half of the cobalt is present as (Co,Mg)O solid solution and the rest exists as $Co_3O_4$, as characterized by Raman spectroscopy and $H_2$-TPR. The catalyst exhibited much higher and stable activity for the $N_2O$ decomposition compared with the 20Co/Al without MgO modification.

## Graphical Abstract

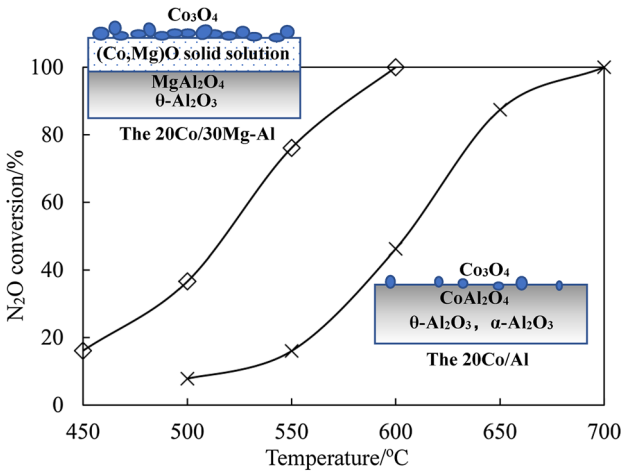


$N_2O$ conversion over the 20Co/30Mg-Al (◇) and the 20Co/Al (×)

**Keywords** MgO · Modification · $Al_2O_3$ support · $Co_3O_4$ · $N_2O$ decomposition

## 1 Introduction

Nitrous oxide ($N_2O$) is the third most significant anthropogenic greenhouse gas and the largest stratospheric-ozone-depleting substance [1, 2]. Nitric and adipic acids plants are the primary industrial contributors emitting this pollutant gas [3]. Several after-treatment technologies to control of $N_2O$ emission was developed, in which catalytic decomposition of the $N_2O$ is most promising, due to its simplicity, high efficiency, and low energy requirements [1, 2].

✉ Xinping Wang
dllgwxp@dlut.edu.cn

[1] State Key Laboratory of Fine Chemical, School of Environmental Science and Technology, Dalian University of Technology, Dalian 116024, China

To eliminate the $N_2O$ emitted from nitric acid plants in this approach, a large number of catalysts have been investigated, such as simple and mixed oxides [4–7], spinels [8–10], perovskites [11, 12], zeolites [13, 14] as well as supported oxides [15–19]. In recent years, spinel-type oxides with the chemical formula $AB_2O_4$ (where A = Mg, Ca, Mn, Co, Ni, Cu, Cr, Fe, Zn and B = Cr, Fe, Co) as the $N_2O$ decomposition catalyst have attracted increasing interest, due to their adequate thermal stability and catalytic activity [20]. Among the spinel-type oxides, cobalt spinels are the most promising generic materials for catalyzing the reaction [8]. Russo et al. [20] found that the spinels, $MgCo_2O_4$, $ZnCo_2O_4$ and $Co_3O_4$, with Co at the B sites exhibit high catalytic activity. Stelmachowski et al. [21] explored the impact arisen from the replacement of both the $Co^{2+}$ cation at the tetrahedral A site and the $Co^{3+}$ cations at the octahedral B sites in $Co_3O_4$ by non-redox $Mg^{2+}$ and $Al^{3+}$ cations by means of experimental and theoretical studies, further proposed that the $N_2O$ decomposition is primarily catalyzed by the octahedral $Co^{3+}$ ions, whereas the tetrahedral $Co^{2+}$ ion is essentially less active to the reaction.

Despite the high catalytic activity, the $Co_3O_4$ in the bulk form is limited for practical applications due to its insufficient mechanical stability and high cost. These drawbacks may be overcome by the dispersion of the spinel over a cheap and mechanically robust carrier. In this regard, there are several investigations in literature concerning the dispersion of the cobalt spinel on alumina [15], zirconia [16], ceria [17] or even on metallic monoliths [19].

Although alumina was widely known to be one of the industrial catalysts supports due to its easy availability, large surface, advantageous mechanical properties, facile processing and shaping [22], its strong interaction with the cobalt oxides is much undesirable. As the interaction at high temperature leads to Co ions occupying the inactive A sites i.e. results in the formation of $CoAl_2O_4$ [23] that is less active for the $N_2O$ decomposition, how to maintain the active state of $Co_3O_4$ on the alumina support become a challenging topic. Jongsomjit et al. found that co-impregnation of ruthenium and cobalt on $Al_2O_3$ could inhibit the interaction of cobalt oxide with alumina [24], and zirconia is more effective for blocking the cobalt aluminate formation [25]. Based on the studies with and without BaO in the $CoO_x$/$Al_2O_3$–BaO catalysts, Liotta et al. reported that BaO has the function of stabilizing the γ-$Al_2O_3$ phase and suppressing solid state diffusion of $Co^{2+}$ ions into alumina bulk phase [26, 27]. Grzybek et al. have found that $Co(NO_3)_2$ precursor is more favorable than $CoCl_2$ for the cobalt maintaining the active state, $Co_3O_4$, when supported on alumina and calcined at 600 °C [28]. They have also found that for the cobalt oxide, using α-$Al_2O_3$ as support is beneficial to maintain its active state, though the alumina in other phases (γ-, δ- and θ-$Al_2O_3$) give rise to high dispersion of the cobalt [22]. However, in the case of α-$Al_2O_3$ loading cobalt oxide, the catalyst surface is greatly sacrificed.

The problem that the strong interaction between active species and the support made the activity of the catalyst largely decrease is also exist in the case of alumina loading other transitional oxides. For instance, the NiO/γ-$Al_2O_3$ catalyst used for methane combustion is suffered from the inactive $NiAl_2O_4$ formation. Gayán found that when γ-$Al_2O_3$ support was coated with MgO and calcined at 800 °C, a stable $MgAl_2O_4$ spinel layer can be produced on the support surface. Using the composited support loading NiO, can effectively minimize the interaction of NiO with the support [29]. In light of this report, we suppose that the $MgAl_2O_4$ spinel layer on $Al_2O_3$ support would be able to protect the active $Co_3O_4$ from the strong interaction with support. Hence, this paper investigates the physical and chemical structure as well as the catalytic activity of the Co/Mg–Al catalyst for $N_2O$ decomposition, so as to develop a possible industrial meaning catalyst working at higher temperature.

## 2 Experimental

### 2.1 Catalyst Preparation

$Al(OH)_3$ was prepared by adding $NH_3{\cdot}H_2O$ to $Al(NO_3)_3{\cdot}9H_2O$ aqueous solution under drastic stirring, washing the precipitate with distilled water and drying the gel at 110 °C overnight. Based on the $Al(OH)_3$, the following different materials that were used as supports for loading cobalt oxide were respectively obtained. Alumina was obtained by calcining the $Al(OH)_3$ in air at 900 °C for 3 h. The bimetal oxide $x$MgO–$Al_2O_3$, which is denoted as $x$Mg–Al with MgO weight percent $x$%, were prepared by adding $NH_3{\cdot}H_2O$ in dropwise into $Al(OH)_3$ slurry that containing desired amount of $Mg(NO_3)_2{\cdot}6H_2O$ under stirring at 30 °C until the pH of mother liquor reached about 11. The resulting material was then aged for 1 h, washed, dried, and calcined in the same way as that for obtaining the alumina. For a purpose of comparison, magnesium aluminate spinel ($MgAl_2O_4$) was prepared by adding $NH_3{\cdot}H_2O$ into an aqueous solution containing stoichiometric amount of $Mg(NO_3)_2{\cdot}6H_2O$ and $Al(NO_3)_3{\cdot}9H_2O$, washing, drying and calcining the resulted material in the same way.

$Co_3O_4$/$Al_2O_3$, $Co_3O_4$/MgO–$Al_2O_3$ and $Co_3O_4$/MgO catalysts with desired $Co_3O_4$ weight percent ($y$%) were respectively prepared by impregnating $Co(NO_3)_2{\cdot}6H_2O$ on the above mentioned alumina, $x$MgO–$Al_2O_3$ and a commercial MgO (purchased from Dunhuang chemical plant) at room temperature for 24 h, drying and calcining the resulted material respectively at 110 °C overnight and 700 °C for 3 h. The obtained catalysts were represented as $y$Co/Al, $y$Co/$x$Mg–Al and $y$Co/Mg respectively. For instance, the 3Co/10Mg–Al

denotes the catalyst prepared by loading 3 wt% $Co_3O_4$ on the 10 wt%MgO–$Al_2O_3$ support. For comparision, pure $Co_3O_4$ was prepared by precipitation method and calcined at 700 °C for 3 h, according to our previous work [8].

### 2.2 Catalyst Characterization

X-ray powder diffraction (XRD) of the catalysts was carried out on a Rigaku Smartlab 9 X-ray diffractometer with Cu Kα radiation (λ = 1.5406 Å) at 45 kV and 200 mA. The diffractograms were recorded with step of 0.02° and a speed of 8°/min. BET surface area of each sample was measured on Micromeritics ASAP 2020 through the nitrogen adsorption at − 196 °C. Before the measurement, the sample was degassed at 300 °C under vacuum for 10 h. Micro-Raman spectra of the samples were recorded at room temperature using a Thermo Fisher DXR Microscope Raman spectrometer with an excitation wavelength of 532 nm. Diffuse reflectance UV–vis spectra of the samples were recorded on a JASCO V-550 spectrophotometer using $BaSO_4$ as a reference in ambient conditions. Temperature programmed reduction ($H_2$-TPR) was performed on a ChemBET TPR/TPD Chemisorption Analyzer. 0.050 g sample (with the sieve fraction of 40–60 mesh) was pretreated in 30 vol% $O_2$/Ar flow at 500 °C for 10 min and cooled to 100 °C. After that, the $H_2$-TPR profiles were recorded in the 5 vol% $H_2$/Ar flow of 100 mL/min at temperature ramp 10 °C/min.

### 2.3 $N_2O$ Decomposition Tests

$N_2O$ decomposition were conducted in a fixed-bed quartz flow reactor loading 0.200 g of catalyst (40–60 mesh). The catalyst was pretreated in Ar at 700 °C for 30 min and then the gas mixture composed of 2000 ppmv $N_2O$, $O_2$ (5 vol%, when present), $H_2O$ (2 vol. when present), NO (100 ppmv, when present) in Ar was fed into the reactor with a total flow rate of 50 mL/min. The gas composition was analyzed by gas chromatography equipped with porapak Q column (4 m in length and 3 mm in inner diameter) using TCD as detector. Steady-state activity data were recorded at each temperature descending from 700 to 450 °C or at a constant temperature (for measuring the catalyst durability). $N_2O$ conversion was calculated according to the equation

$$\text{Conv.}\% = \frac{c(N_2O)_{in} - c(N_2O)_{out}}{c(N_2O)_{in}} \times 100\%$$

## 3 Results and Discussion

### 3.1 Alumina Modified with Different Amount of Magnesium Oxide

Figure 1 shows XRD patterns of the $Al_2O_3$, the bimetal oxide 10Mg–Al and 30Mg–Al calcined at 900 °C for 3 h. For the $Al_2O_3$, which give a small specific surface area of 18.06 $m^2/g$, it exhibited sharp peaks due to α-$Al_2O_3$ and lower peaks arisen from θ-$Al_2O_3$. Whereas, in the case of 10Mg–Al, which gave a specific surface area of 50.79 $m^2/g$, no peaks ascribed to α-$Al_2O_3$ could be observed. Instead, strong peaks due to $MgAl_2O_4$ phase (JCPDS 21-1152) appeared on the sample. Clearly, it is the $MgAl_2O_4$ formation which suppressed the phase transformation from θ- to α-$Al_2O_3$, though the atomic ratio of Mg/Al is about 0.14 that is much less than the stoichiometric ratio (0.5) of $MgAl_2O_4$. On the 30Mg–Al, the diffraction of $MgAl_2O_4$ became more intensive and besides which some diffraction peaks belong to MgO (JCPDS 43-1022) were appeared. It means that 30 wt% of MgO is enough to produce $MgAl_2O_4$ covering the $Al_2O_3$ surface.

### 3.2 Chemical State of Cobalt in the 3Co/*x*Mg–Al Influenced by the Magnesium Oxide Amount

Figure 2 shows Raman spectra of 3Co/Al, 3Co/10Mg–Al and 3Co/30Mg–Al in comparison with that of $Co_3O_4$. On the $Co_3O_4$, five Raman peaks at 189, 467, 511, 609 and 672 $cm^{-1}$ corresponding to the $E_g$, $3xF_{2g}$ and $A_{1g}$ vibrational modes of the crystalline [30] appeared. On the 3Co/Al, although the first three peaks belong to the $Co_3O_4$ crystalline with a slight blue shift could be confirmed, a splitting band of $A_{1g}$ at about 690 $cm^{-1}$ being associated with the $Al^{3+}$ substituting octahedral $Co^{3+}$ in the spinel structure [28] clearly appeared. It indicates that both of $Co_3O_4$ and $CoAl_2O_4$ exist in the 3Co/Al. Unexpectedly, the band splitting is more evident for the 3Co/10Mg–Al compared with that of the 3Co/Al, which indicates that the transformation of the $Co_3O_4$ to $CoAl_2O_4$ due to the calcination is even more severe for the 3Co/10Mg–Al compared with the 3Co/Al. The same

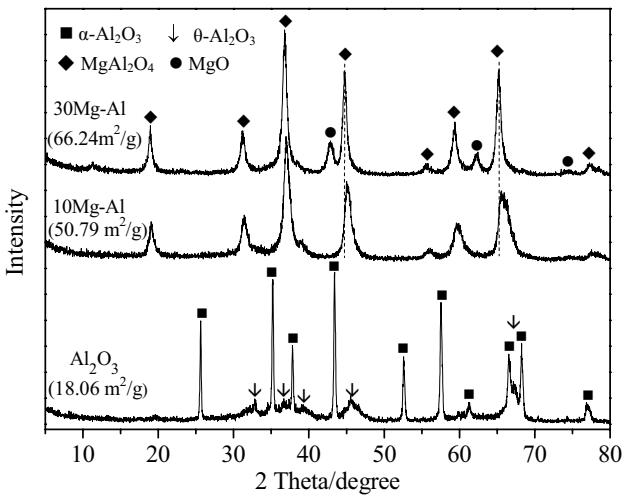


**Fig. 1** XRD patterns of the different supports (the data at the brackets corresponding to the BET surface areas)

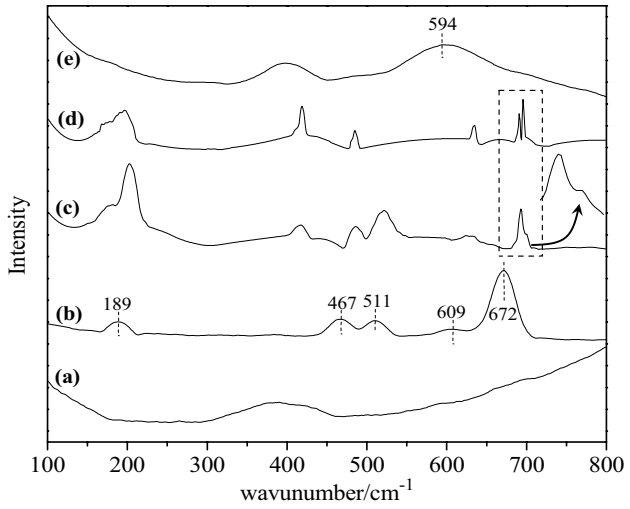


**Fig. 2** Raman spectra of the $MgAl_2O_4$ (**a**), $Co_3O_4$ (**b**), 3Co/Al (**c**), 3Co/10Mg–Al (**d**) and 3Co/30Mg–Al (**e**)

conclusion could be obtained from optical diffuse reflectance spectra of the two samples. As shown in the Fig. 3, the characteristic triplet absorption at 1.97, 2.13 and 2.28 eV due to the spin-forbidden $^4A_2(F) \rightarrow {}^2T_1(G)$, $^2E(G)$, spin-allowed $^4A_2(F) \rightarrow {}^4T_1(P)$, and spin-forbidden $^4A_2(F) \rightarrow {}^2T_2(G)$ transitions for the tetracoordinated $Co^{2+}$ [31] is more remarkable for the 3Co/10Mg–Al compared with that of the 3Co/Al, indicating that there are more $CoAl_2O_4$ existing in the 3Co/10Mg–Al with respect to the 3Co/Al. The more θ-$Al_2O_3$ phase of the 10Mg–Al compared with the $Al_2O_3$ should be responsible for the undesired results. In the case of the $Al_2O_3$ loading $Co_3O_4$ after the calcination, as discussed in the Sect. 3.1, as the alumina primarily exists as α-$Al_2O_3$, it properly inhibited the transformation of the $Co_3O_4$ to $CoAl_2O_4$ [22]. Considering that although all of magnesium in the 10Mg–Al exist as $MgAl_2O_4$, it could not effectively protect the cobalt from transforming to the $CoAl_2O_4$, 30Mg–Al was investigated as the support to load cobalt oxide. As shown in the Fig. 2, no Raman bands belong to either $CoAl_2O_4$ or $Co_3O_4$ were observed on the 3Co/30Mg–Al, and instead, two broad absorption bands respectively appeared at about 398 $cm^{-1}$ and 594 $cm^{-1}$. The former band can be ascribed to that of $MgAl_2O_4$, because the $MgAl_2O_4$ gave the same band at 398 $cm^{-1}$ (a, in Fig. 2). Furthermore, it is strongly supported by the literature [32]. For the band at about 594 $cm^{-1}$, it can be ascribed to solid solution of (Co,Mg)O, which will be discussed in details below.

It has been reported that the solid solution (Co,Mg)O (JCPDS 02-1201) can be formed from solid-state reaction of cobalt oxide with magnesium oxide [33]. It was confirmed by the XRD of the MgO and 20Co/Mg samples, as shown in the Fig. 4. On the 20Co/Mg, the diffraction peaks arisen from MgO (or composite metal oxides) clearly shifted to lower angles compared with that of the pure MgO (refer to the insert). For instance, the strongest peak arising from the (2 0 0) reflection for the pure MgO at 42.90° shifted to 42.83° for the 20Co/Mg, corresponding to the $Co^{2+}$ with larger radius (74 pm) replacing the $Mg^{2+}$ with smaller radius (65 pm). Figure 5 shows the Raman spectra of the 3Co/Mg and 20Co/Mg samples. It can be seen that the broad band similar to that of the 3Co/30Mg–Al but centered at 579 $cm^{-1}$ appeared on the both samples and that the intensity of the peak increased with the Co content increasing. These results clearly confirmed that the broad band at about 579 $cm^{-1}$ is characteristic of the cobalt in the (Co,Mg)O phase. Hence, the broad band at about 594 $cm^{-1}$ observed on the 3Co/30Mg–Al can be reasonably assigned to the cobalt in (Co,Mg)O solid solution.

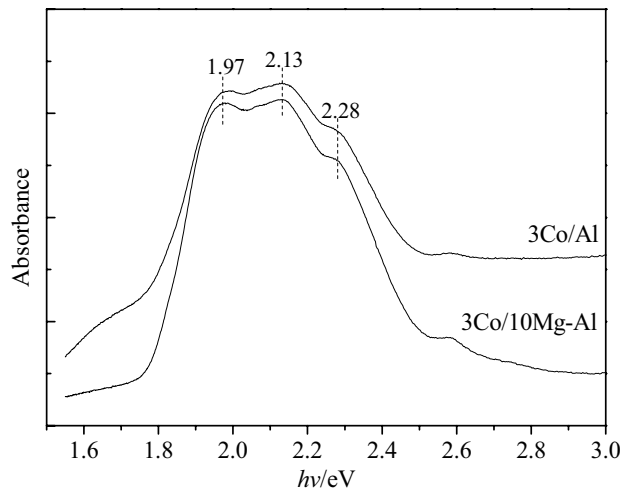


**Fig. 3** The optical diffuse reflectance spectra of the 3Co/Al and 3Co/10Mg–Al

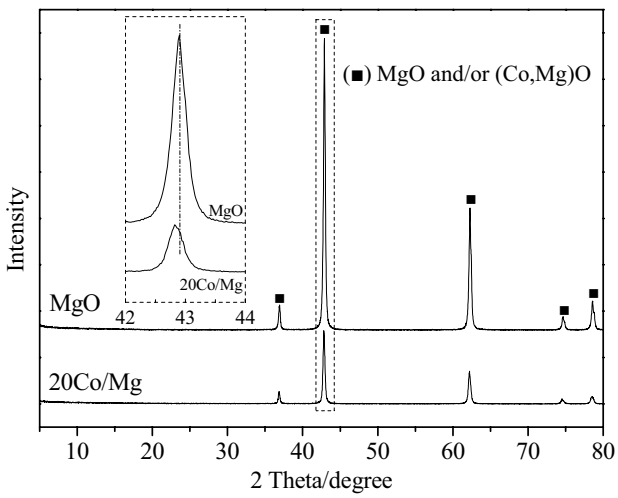


**Fig. 4** XRD patterns of the MgO and 20Co/Mg. The insert magnifies the most intensive diffraction peak of the two samples

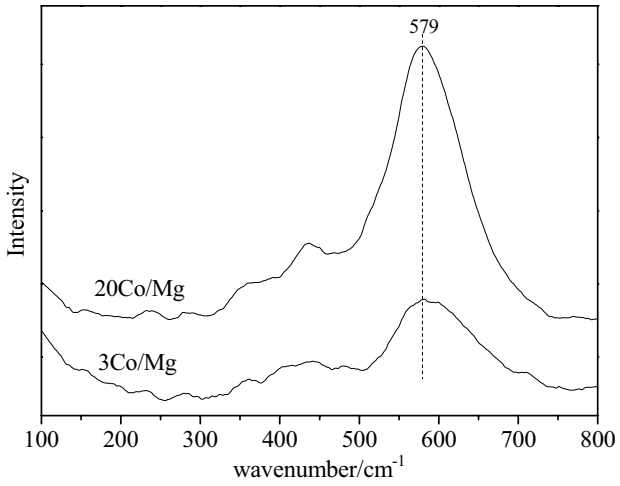


**Fig. 5** Raman spectra of the 3Co/Mg and 20Co/Mg

The catalytic activities of the 3Co/*x*Mg–Al ($x=0$, 10, 20, 30) with the same cobalt loading amount (3 wt% $Co_3O_4$) are compared (Fig. 6). It generates the activity order 3Co/30Mg–Al > 3Co/20Mg–Al > 3Co/Al > 3Co/10Mg–Al. Clearly, the order can be interpreted well by the primary chemical state of cobalt in the catalysts. The small amount (10 wt%) of MgO addition to the $Al_2O_3$ support led to marked decrease of the activity, which is associated with the more inactive $CoAl_2O_4$ formation in the 3Co/10Mg–Al. Interestingly, 30 wt% of MgO addition to the $Al_2O_3$ support made the activity of the corresponding catalyst significantly increased. It is in line with the formation of (Co,Mg)O instead of that of $CoAl_2O_4$ in the catalyst, as discussed afore (in Raman spectroscopy). No further activity increasing was observed when the more MgO was used for modifying the $Al_2O_3$ support, which may be resulted from the large surface area losing of the corresponding catalysts.

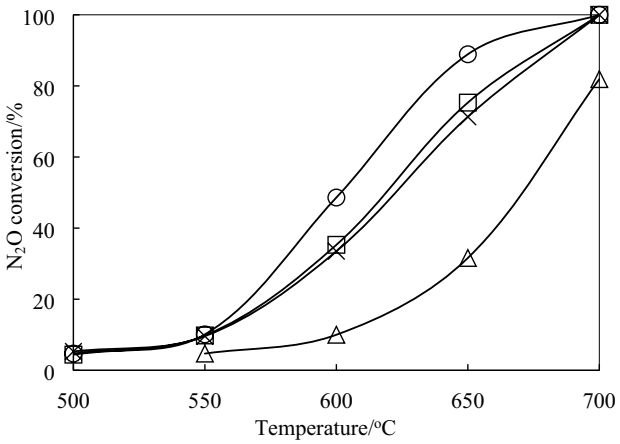


**Fig. 6** $N_2O$ conversion over the 3Co/*x*Mg–Al: (multiple sign) $x=0$, (open triangle) $x=10$, (open square) $x=20$, (open circle) $x=30$

Herein, a recent report given by Klegová et al. [18] should be noticed, who compared 70%MgO/30%$Al_2O_3$ and 30%MgO/70%$Al_2O_3$ loading definite amount of $Co_3O_4$ (25.2 wt% accounted in Co), in which the $Al_2O_3$ was used as binder to benefit the support shaping, and found that the $Co_3O_4$/70%MgO/30%$Al_2O_3$ catalyst is more active than the counterpart for the $N_2O$ decomposition. Their results also significantly indicate that the cobalt on the MgO surface is more active than that on the $Al_2O_3$ surface.

### 3.3 Impact of the Magnesium Oxide on the Activity of the 20Co/30Mg–Al

Figure 7a shows the activity variation of the catalysts with the $Co_3O_4$ loading amount change on the 30Mg–Al. With the $Co_3O_4$ loading amount increase in the range of 3–20 wt%, the $N_2O$ conversion over the catalysts at each reaction temperature greatly increased. However, no significant increase in the $N_2O$ conversion could be observed when the $Co_3O_4$ loading amount was further increased to 30 wt%, which may be resulted from the surface area losing of the 30Co/30Mg–Al (42.75 $m^2$/g) with respect to the 20Co/30Mg–Al (52.93 $m^2$/g). Based on the results, specific reaction rates of the $N_2O$ decomposition over the

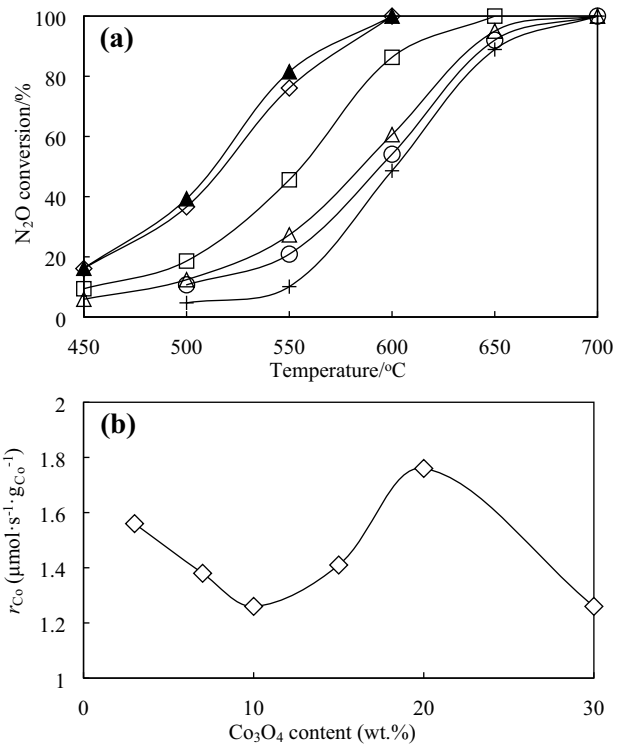


**Fig. 7** **a** $N_2O$ conversion over the *y*Co/30Mg–Al: (plus sign) $y=3$, (open circle) $y=7$, (open triangle) $y=10$, (open square) $y=15$, (open diamond) $y=20$, (filled triangle) $y=30$; **b** The specific reaction rates of the $N_2O$ decomposition over the *y*Co/30Mg–Al catalysts at 550 °C in unit amount of Co ($r_{Co}$)

*y*Co/30Mg–Al catalysts at 550 °C in unit amount of Co were calculated (Fig. 7b), from which it is can be known that the 20Co/30Mg–Al gives an outstanding large $N_2O$ decomposition specific reaction rate in the unit amount of Co among the catalysts with different $Co_3O_4$ loadings. It indicates that the cobalt component in the 20Co/30Mg–Al works in the highest effectiveness for catalyzing the reaction among the catalysts. From the Raman spectrum (Fig. 8), it can be known that part of cobalt exists as (Co,Mg)O solid solution, as discussed in the Sect. 3.2, and the rest exists as $Co_3O_4$ phase in the 20Co/30Mg–Al. Thus, for the *y*Co/30Mg–Al catalysts, the $N_2O$ decomposition specific reaction rates over them changed with the $Co_3O_4$ loading amount could be explained as follows. When the cobalt oxide loading amount increased in the *y*Co/30Mg–Al in the percent $y = 3–10$, the cobalt is primarily present in (Co,Mg)O solid solution, and the average depth of the cobalt location in the solid solution increases, which negatively influences the specific reaction rate. Whereas, when the $Co_3O_4$ loading amount further increased, for instance, from 10 wt% to 20 wt%, the $Co_3O_4$ species that is more active than the (Co,Mg)O for the reaction begins to be produced, which interprets why the 20Co/30Mg–Al gives the much higher specific reaction rate compared to the *y*Co/30Mg–Al with lower $Co_3O_4$ loading amounts. Based on the above discussion, the chemical structure of the 20Co/30Mg–Al can be schematically represented in Fig. 9.

Figure 10 shows $H_2$-TPR profiles of the 20Co/30Mg–Al comparing with those of 20Co/Al and the bulk $Co_3O_4$ sample. Two hydrogen consumption peaks at 401 and 440 °C appeared on the bulk $Co_3O_4$ sample, which could be respectively ascribed to the reduction of $Co^{3+}$ to $Co^{2+}$ and $Co^{2+}$ to $Co^0$ [17]. However, on the 20Co/Al, the peaks markedly shifted to about 486 and 563 °C and the hydrogen consumption below 440 °C was almost negligible. It reveals that the cobalt in the 20Co/Al is predominantly present as $CoAl_2O_4$ [23], which is in agreement with that measured by Raman spectroscopy (Fig. 8). Interestingly, it can be found from the figure, that the primary hydrogen consumption peak over the 20Co/30Mg–Al appeared at 395 °C that is even lower than those on the bulk $Co_3O_4$ sample. The result indicates that the oxygen ions of the $Co_3O_4$ species in the 20Co/30Mg–Al are more active towards reduction, i.e. Co–O bond in the $Co_3O_4$ species is weaker in somewhat compared with that in the bulk $Co_3O_4$ sample. For the transitional based catalysts, it has been documented that their active sites regeneration concerning the Co–O bond rupture controls $N_2O$ decomposition over the catalysts [2]. Thus, the activity of the active sites must be reflected by temperature of the reduction peak in the $H_2$-TPR. In Fig. 10, it can be also found that the area of the reduction peak for the 20Co/30Mg–Al below 470 °C is about half of the bulk $Co_3O_4$. The results indicate that the corresponding portion of the cobalt is present as $Co_3O_4$ species in the 20Co/30Mg–Al while the rest exists in the state that hardly reduced by $H_2$, which is in good consistent with that measured by Raman spectroscopy (Fig. 8) and supports the chemical structure of the 20Co/30Mg–Al catalyst illustrated in Fig. 9.

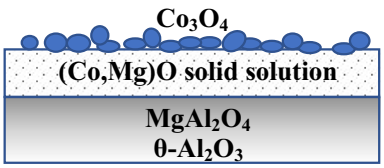


**Fig. 9** The scheme of the chemical structure of the 20Co/30Mg–Al

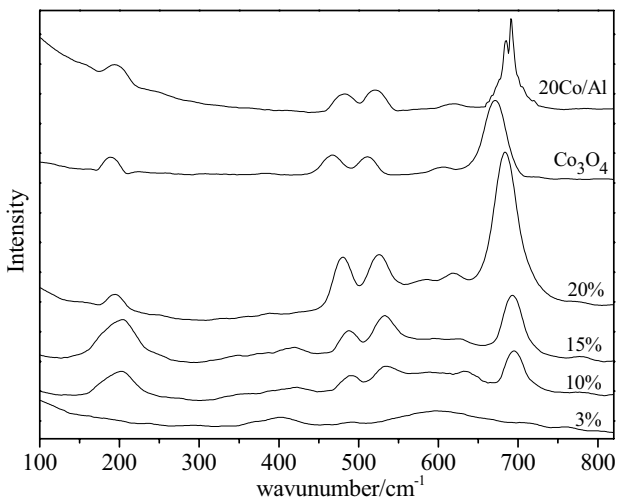


**Fig. 8** Raman spectra of the *y*Co/30Mg–Al ($y = 3–20$), 20Co/Al and $Co_3O_4$

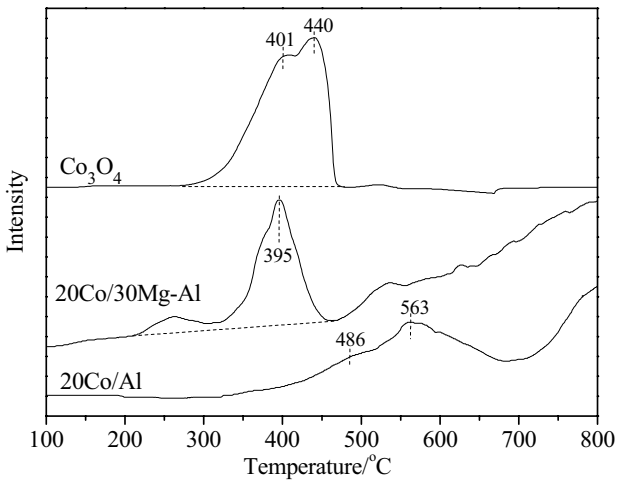


**Fig. 10** $H_2$-TPR profiles of the 20Co/30Mg–Al, 20Co/Al and $Co_3O_4$ (calcined at 700 °C) normalized in cobalt amount

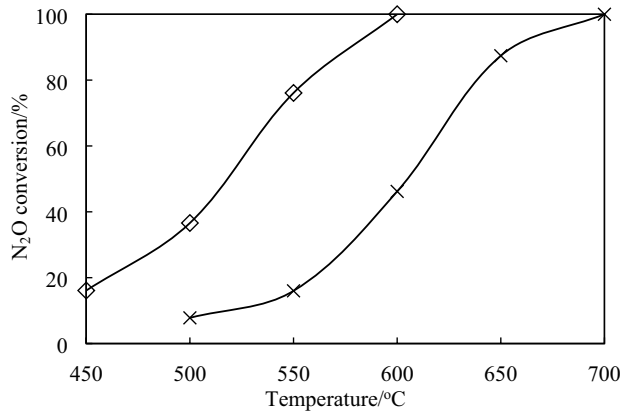


**Fig. 11** $N_2O$ conversion over the 20Co/30Mg–Al (open diamond) and the 20Co/Al (multiple sign)

As expected, the 20Co/30Mg–Al exhibited much higher activity at each reaction temperature compared with the 20Co/Al (Fig. 11). For instance, the 20Co/30Mg–Al at 550 °C gave the $N_2O$ conversion of 76% that is about 5 times as high as that of the 20Co/Al under the same reaction conditions.

### 3.4 Catalytic Performance of the 20Co/30Mg–Al

Figure 12 shows the $N_2O$ decomposition results of 2000 ppmv $N_2O$ in the presence of some impurities over the 20Co/30Mg–Al catalyst. For the 2000 ppmv $N_2O$ in Ar, the $N_2O$ was completely decomposed at 600 °C. 100 ppmv NO and 5% $O_2$ existing in the gas stream just made the temperature for the complete $N_2O$ decomposition over the catalyst shifted from 600 to 650 °C. In the figure, it can be found that, the impurity gas giving the largest impact on the catalytic activity among the 100 ppmv NO, 5 vol% $O_2$ and 2 vol% $H_2O$ is the 2 vol% $H_2O$. Nevertheless, the 20Co/30Mg–Al catalyst still completely eliminated the $N_2O$ at 700 °C under the most severe condition of the three impurity gases coexisting in the gas stream.

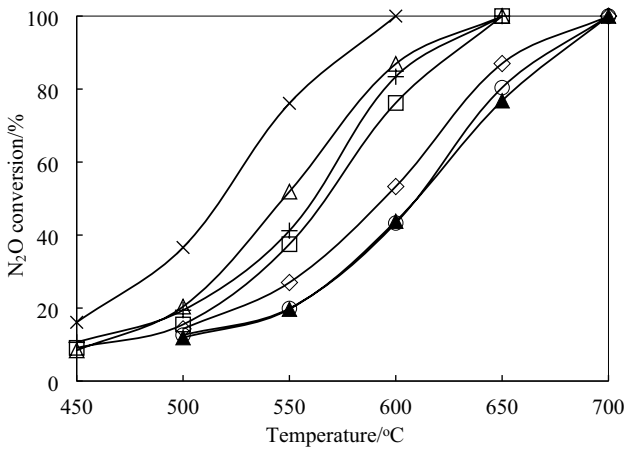


**Fig. 12** $N_2O$ conversion over the 20Co/30Mg–Al for the feed gas 2000 ppmv $N_2O$/Ar (multiple sign) in the presence of 100 ppmv NO (open triangle), 5 vol% $O_2$ (plus sign), 100 ppmv NO + 5 vol% $O_2$ (open square), 2 vol% $H_2O$ (open diamond), 2 vol% $H_2O$ + 5 vol% $O_2$ (open circle) or 2 vol% $H_2O$ + 100 ppmv NO + 5 vol% $O_2$ (filled triangle)

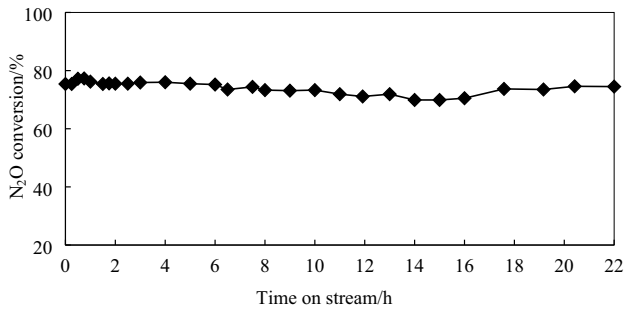


**Fig. 13** $N_2O$ conversion over the 20Co/30Mg–Al at 550 °C changed with time on stream of 2000 ppmv $N_2O$/Ar

To estimate the industrial potential of using the 20Co/30Mg–Al catalyst processes the $N_2O$ by decomposition, the durability of the catalyst was tested at 550 °C. As shown in Fig. 13, there was no obvious evidence of catalytic activity lost in the time on stream of 22 h for the catalyst in the 2000 ppmv $N_2O$/Ar, thereby demonstrated that the catalyst has stable catalytic activity for the $N_2O$ decomposition.

## 4 Conclusions

Using the support of alumina modified with MgO to load $Co_3O_4$, can effectively avoid undesired $CoAl_2O_4$ formation at high temperature (700 °C) as long as the adequate amount of MgO (ca. 30 wt%) was used in the modification. The modification was realized by depositing $Mg(OH)_2$ on $Al(OH)_3$ and calcining the resulted material at 900 °C. For the 20Co/30Mg–Al catalyst, which was prepared by modifying alumina with 30 wt% MgO and loading 20 wt% $Co_3O_4$ on the composited support, about half of the cobalt exists as (Co,Mg)O solid solution and the rest exists as $Co_3O_4$ in the catalyst. Almost no $CoAl_2O_4$ was produced even though the catalyst had been subjected to the calcination at 700 °C for 3 h. Hence, the catalyst has much higher and stable activity for the $N_2O$ decomposition compared with the 20Co/Al that contains the same amount of cobalt with that of the 20Co/30Mg–Al but without MgO modifying the alumina.

**Acknowledgements** This work was financially supported by the National Natural Science Foundation of China (Grant Nos. 21277019 and 21777015).

## References


1. Pérez-Ramírez J, Kapteijn F, Schöffel K, Moulijn JA (2003) Appl Catal B 44:117–151
2. Konsolakis M (2015) Acs Catal 5:6397–6421
3. Lee SJ, Ryu IS, Kim BM, Moon SH (2011) Int J Greenh Gas Con 5:167–176
4. Ohnishi C, Asano K, Iwamoto S, Chikama K, Inoue M (2007) Catal Today 120:145–150
5. Stelmachowski P, Zasada F, Piskorz W, Kotarba A, Paul JF, Sojka Z (2008) Catal Today 137:423–428
6. Zhang FF, Wang XP, Zhang XX, Turxun M, Yu HB, Zhao JJ (2014) Chem Eng J 256:365–371
7. Zabilskiy M, Erjavec B, Djinović P, Pintar A (2014) Chem Eng J 254:153–162
8. Yu HB, Tursun M, Wang XP, Wu XX (2016) Appl Catal B 185:110–118
9. Abu-Zied BM, Soliman SA, Abdellah SE (2015) J Ind Eng Chem 21:814–821
10. Yu HB, Wang XP, Wu XX, Chen Y (2018) Chem Eng J 334:800–806
11. Ivanov DV, Sadovskaya EM, Pinaeva LG, Isupova LA (2009) J Catal 267:5–13
12. Wu Y, Ni X, Beaurain A, Dujardin C, Granger P (2012) Appl Catal B 125:149–157
13. Ates A (2014) Catal Sci Technol 4:2031–2041
14. da Cruz RS, Mascarenhas AJS, Andrade HMC (1998) Appl Catal B 18:223–231
15. Gudyka S, Grzybek G, Grybos J, Indyka P, Leszczynski B, Kotarba A, Sojka Z (2017) Appl Catal B 201:339–347
16. Pietrogiacomi D, Campa MC, Carbone LR, Tuti S, Occhiuzzi M (2016) Appl Catal B 187:218–227
17. Grzybek G, Stelmachowski P, Gudyka S, Indyka P, Sojka Z, Guillén-Hurtado N, Rico-Pérez V, Bueno-López A, Kotarba A (2016) Appl Catal B 180:622–629
18. Klegová A, Pacultová K, Fridrichová D, Volodarskaja A, Kovanda F, Jirátová K (2017) Chem Eng Technol 40:981–990
19. Boissel V, Tahir S, Koh CA (2006) Appl Catal B 64:234–242
20. Russo N, Fino D, Saracco G, Specchia V (2007) Catal Today 119:228–232
21. Stelmachowski P, Maniak G, Kaczmarczyk J, Zasada F, Piskorz W, Kotarba A, Sojka Z (2014) Appl Catal B 146:105–111
22. Grzybek G, Ciura K, Wójcik S, Gryboś J, Indyka P, Inger M, Antoniak-Jurak K, Kowalik P, Kotarba A, Sojka Z (2017) Catal Sci Technol 7:5723–5732
23. Ji YG, Zhao Z, Duan AJ, Jiang GY, Liu J (2009) J Phys Chem C 113:7186–7199
24. Jongsomjit B, Panpranot J, Goodwin JG Jr (2001) J Catal 204:98–109
25. Jongsomjit B, Panpranot J, Goodwin JG Jr (2003) J Catal 215:66–77
26. Liotta LF, Pantaleo G, Macaluso A, Di Carlo G, Deganello G (2003) Appl Catal A 245:167–177
27. Liotta LF, Pantaleo G, Di Carlo G, Marcì G, Deganello G (2004) Appl Catal B 52:1–10
28. Grzybek G, Wójcik S, Ciura K, Gryboś J, Indyka P, Oszajca M, Stelmachowski P, Witkowski S, Inger M, Kotarba A, Sojka Z (2017) Appl Catal B 210:34–44
29. Gayán P, de Diego LF, García-Labiano F, Adánez J, Abad A, Dueso C (2008) Fuel 87:2641–2650
30. Hadjiev VG, Iliev MN, Vergilov IV (1988) J Phys C 21:L199–L201
31. Keppler H, Bagdassarov N (1999) Chem Geol 158:105–115
32. Kushwaha AK (2010) Phys B 405:2795–2798
33. Wang HY, Ruckenstein E (2001) Appl Catal A 209:207–215